University of Bath

Alternative formats
If you require this document in an alternative format, please contact:
openaccess@bath.ac.uk

STRATIFIED AND BUOYANCY-INDUCED FLOW IN CLOSED COMPRESSOR ROTORS

Gary D. Lock   **Richard W. Jackson**   **Mikolaj Pernak**   **Oliver J. Pountney**

Carl M. Sangan   **J. Michael Owen**   **Hui Tang***   **James A. Scobie**

Department of Mechanical Engineering
University of Bath
Bath, BA2 7AY
United Kingdom
*E-mail: h.tang2@bath.ac.uk

ABSTRACT

The radial growth of compressor discs is strongly influenced by conjugate heat transfer between conduction in the co-rotating discs and buoyancy-driven convection in the rotating fluid core between the discs. An accurate prediction of metal temperatures of these discs is an important issue in thermo-mechanical design, where blade-tip clearances must be controlled carefully to ensure safety and efficiency under all operating conditions. This paper presents an experimental study of the fluid dynamics and heat transfer in a closed rotating cavity, comparing results with theoretical models and introducing a new compressibility parameter χ. At large values of χ, where compressibility effects are significant, the air temperature approaches that of the shroud; such conditions suppress buoyancy effects and the flow in the rotating cavity becomes stratified, with convection replaced by conduction inside the fluid core. There are important practical consequences of stratification with significant differences in temperature distributions and stresses inside compressor discs.

The influence of χ is also shown on the radial temperature distributions for the discs and on the shroud heat transfer correlations, which are compared qualitatively with previously published data collected where the effects of compressibility are relatively small. The experiments reveal that there is a critical value of χ where the convective heat flux to the shroud is zero. The radial distribution of disc temperature was that expected from pure conduction in a cylinder. A new heat transfer correlation based on measured shroud heat flux and the theoretical core temperature is presented.

The unsteady flow characteristics in the cavity were also investigated, identifying coherent rotating structures across a range of experimental conditions. These cyclonic / anti-cyclonic vortex pairs generate the non-dimensional circumferential pressure difference necessary for the radial outflow (of cold fluid) and inflow (of hot fluid) through the rotating core. The experiments show the magnitude of these pressure variations can be correlated against Grashof number and that at high values of χ the structures do not exist. The combined experimental and theoretical results will be of practical interest to engine designers and for the validation of computational models.

1 INTRODUCTION

It is now urgent to significantly reduce harmful emissions at altitude to avoid catastrophic climate change. The next generation of aero-engines (*e.g.* ultra-high-bypass ratio, geared turbofans and hybrid-electric systems) have technology drivers demanding smaller core dimensions; these require shorter compressor blades with increased sensitivity to clearance losses and reliability across a flight cycle. To enable new technologies and architectures, engine designers must predict the temperature and radial growth of compressor discs (to which the blades are attached), which affect the blade tip clearance and compressor stability. These design issues are particularly acute during engine transients.

Efficient operation with reduced fuel consumption is dependent on high turbine entry temperatures, which lead to the requirement of secondary air systems (SAS) that divert air from the compressor for cooling purposes. A generic cross-section of an aero-engine compressor with co-rotating discs, cobs, cavities, internal shaft, and flow paths is shown in Figure 1. Heat is transferred to the shrouds and discs from the hot, compressed air in the main gas path, while a relatively cool axial throughflow passes through the annular gap between the disc cobs and the shaft. Under cruise conditions, the shroud is hotter than the throughflow and *buoyancy-induced flow* can occur in the open rotating cavities formed by the discs and shroud. However, at other points in the flight cycle the shroud can become colder than the cob, and this suppresses buoyancy effects; here *stratified flow* may form with heat transfer governed by conduction rather than convection. The radial distribution of temperature and thermal stress in the discs determine the expansion of the rotor and the running clearance between the compressor blades and the outer casing in the mainstream cavity. The issue is also pertinent to industrial gas turbines, where the
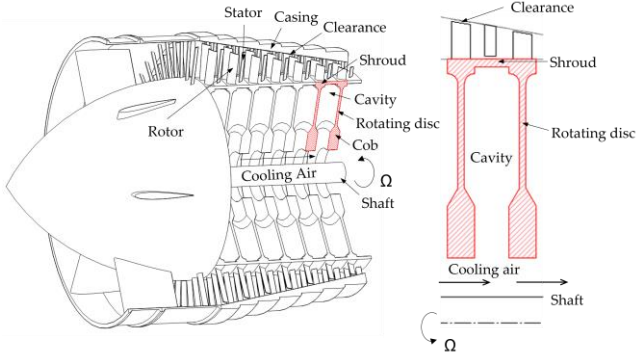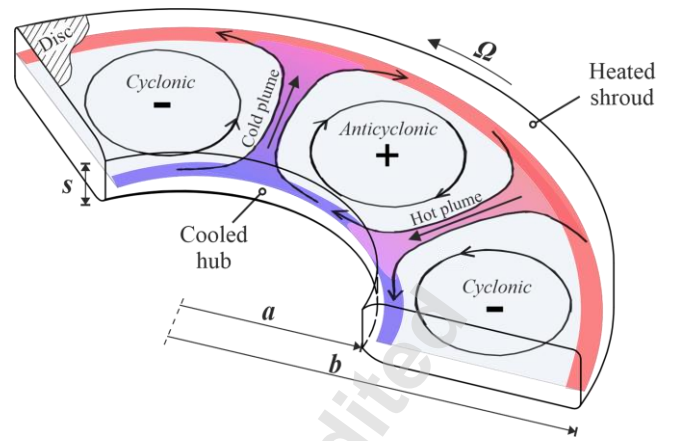
Figure 1: Aero-engine compressor cavity [1].

cobs can be contiguous, essentially forming a *closed rotating compressor cavity*. Buoyancy-induced flow is a strongly conjugate problem: the temperature distribution on the discs affects the flow in the cavity, and vice-versa.

Buoyancy-induced flow in closed stationary cavities

Rayleigh-Bérnard convection [2] occurs in a fluid between horizontal plates in a gravitational field, where the heat transfer is governed by the Rayleigh number (Ra):

$$Ra \overset{\text{def}}{=} Pr \, \beta \Delta T \frac{gL^3}{\nu^2} \quad (1)$$

Here Pr is the ratio of kinematic viscosity to thermal diffusivity of the fluid, L is the vertical separation of the plates at a temperature difference of ΔT - other symbols are defined in the nomenclature. If a fluid layer is heated from below and cooled from above, the driving force for thermal convection is the buoyancy. Cold, dense fluid is above warmer, lighter fluid; at a critical Rayleigh number of 1708 a parcel of fluid will rise when the buoyancy force is able to overcome viscosity. Below this critical number, heat transfer is by conduction.

Coriolis effects in a closed rotating annulus

Consider fluid in a cylindrical cavity with cooled inner and heated outer walls under near solid-body rotation Ω as illustrated in Figure 2. This geometry models the closed rotating compressor cavity described above: the inner wall is the *hub* (or closed cobs) at radius a and the outer wall the *shroud* at radius b; the cavity is bounded by the two rotating discs with spacing s and the radial temperature gradient creates buoyancy-induced flow. Unlike natural convection in a gravitational field, radial flow can only occur by two mechanisms: either it must be confined to the viscous boundary layers on the rotating discs (Ekman layers), where the Coriolis forces are produced by shear stresses; or the inviscid core must be non-axisymmetric where cyclonic and anti-cyclonic circulation produce circumferential pressure gradients that create the Coriolis forces. The heat transfer process is analogous to the Rayleigh-Bérnard convection described above with g replaced by the centripetal acceleration $\Omega^2 r \gg g$. The shroud heat transfer is usually characterised by the Nusselt and Grashof numbers:

Figure 2: Rotating annulus model of a closed compressor cavity

$$Nu \overset{\text{def}}{=} \frac{qL}{k\Delta T} \quad (2)$$

$$Gr \overset{\text{def}}{=} Re_\phi^2 \frac{L}{r} \beta \Delta T \quad (3)$$

where Re_ϕ is the rotational Reynolds number and

$$Ra = Gr Pr \quad (4)$$

$$Re_\phi = \frac{\rho \Omega r L}{\mu} \quad (5)$$

These are generic definitions at radius r, temperature difference ΔT and length scale L related to dimensions a, b and s; the specific definitions for Nu, Re_ϕ and Gr appropriate for the experimental conditions presented in this paper are discussed below and in Section 4. In aero-engines, Gr is $O(10^{13})$ assuming $L = b$, Re_ϕ $O(10^7)$ and $\beta\Delta T$ $O(10^{-1})$.

Heat transfer and flow structure in a closed rotating annulus

Bohn *et al.* [3] (the Aachen group) published a series of experimental and computational papers related to three closed cylindrical rotating cavities modelling an aero-engine compressor. Using the definitions related to Figure 2, one of the cavities was an air-filled closed cavity with dimensions a, b and s being 0.125 m, 0.24 m and 0.12m respectively; this gives radius and gap ratios $a/b = 0.52$ and $G = s/b = 0.5$. The shroud was heated and the hub cooled, with the two discs insulated to create quasi-adiabatic boundaries. In the absence of heat transfer from the discs, the total heat flow rates through the inner and outer surfaces were assumed equal and the Nusselt number calculated as the ratio of this heat flux to that measured by conduction. The definition of the Rayleigh and Reynolds number used by Bohn *et al.* are as follows:

$$Ra_B = Pr Gr_B = Pr Re_B^2 \frac{2(b-a)}{b+a} \beta \Delta T \quad (6)$$

$$Re_B = \frac{\Omega(b^2 - a^2)}{2\nu} \quad (7)$$

$$\text{Nu}_B = \frac{q_b}{q_c} \text{ where } q_c = \frac{k\Delta T}{b \ln\left(\frac{b}{a}\right)} \tag{8}$$

Here $\Delta T = T_b - T_a$ is the difference in temperatures between the shroud and hub, q_b and q_c are the heat fluxes at the shroud and due to conduction, respectively. Using these definitions, the following empirical correlation was established over the range $10^7 < \text{Ra}_B < 10^{12}$ and $\beta\Delta T < 0.3$:

$$\text{Nu}_B = 0.317\,(\text{Ra}_B)^{0.211} \tag{9}$$

Tang and Owen [4] successfully modelled these shroud heat transfer correlations by assuming the cylindrical surfaces were equivalent to horizontal plates experiencing laminar free convection, but with the gravitational acceleration replaced by the centripetal acceleration. They showed the exponent in eq. 9 was less than 0.25, the value associated with laminar free convection, due to compressibility of the air in the rotating cavity. It might seem surprising that laminar buoyancy models are appropriate at the high rotational speeds experienced inside the compressors of aero-engines; however, the large Coriolis accelerations will attenuate turbulence in the fluid core and the differences between the rotational speed of the core (near solid-body rotation) and the discs is relatively small.

Pitz *et al.* [5] simulated flow and heat transfer in the same cavity using an incompressible Direct Numerical Simulation (DNS); in all cases the computed Nu_B-Ra_B correlations were in good agreement with the experiments conducted by Holland *et al.* [6] and Niemela *et al.* [7], and the theoretical results of Grossmann and Lohse [8], all for non-rotating systems. Pitz *et al.* [9] simulated the same cavity using incompressible Large-Eddy Simulation (LES), showing laminar Ekman layer behaviour over the range $10^7 < \text{Ra}_B < 10^9$. Gao *et al.* [10] compared disc boundary layer profiles calculated from three-dimensional incompressible DNS and compressible LES codes for the Aachen cavity, further confirming laminar Ekman layer behaviour. The calculated Nusselt numbers lay above those measured at Aachen but the exponent of the Nu_B-Ra_B correlation from the LES results (0.286) agreed well with the exponent corrected by Bohn and Gier [11] (0.297); a similar exponent was determined by Saini *et al.* [12] using a compressible DNS solver. Jackson *et al.* [13] presented radial distributions of disc temperature and heat flux using the Bath Compressor Cavity Rig in a closed-cavity configuration. Unlike the Aachen rig (where the discs were quasi-adiabatic) there was significant heat transfer from the disc surfaces; shroud heat transfer correlations were not produced as there was no measurement or calculation of the core temperature.

In terms of flow structure, both Pitz *et al.* [9] and Gao *et al.* [10] computed either four or five pairs of counter-rotating vortices over the range $10^7 < \text{Ra}_B < 10^9$ for the Aachen rig. Jackson *et al.* [13] used unsteady pressure sensors to detect either three or four vortex pairs in the rotating core; the number of pairs changed with Grashof number, with the fluid core slipping relative to the rotating discs by $< 1\%$ of the disc speed.

Owen [14] suggested that the number of vortex pairs (or the self-organising flow structure) was associated with the maximum production of entropy. He assumed circular vortices in the cavity and predicted that the number of vortex pairs was related by:

$$\frac{a}{b} = \frac{2n - \pi}{2n + \pi} \tag{10}$$

where n is the number of vortex pairs. Pitz *et al.* [15] calculated the flow structures in different closed cavity geometries using linear stability analysis and the calculated numbers of vortex pairs agreed with eq. 10.

Theoretical and experimental models of physical systems

Understanding the buoyancy-induced rotating flow requires the involvement of physicists and mathematicians as well as engineers. This paper uses both theoretical and experimental models to investigate the flow and heat transfer in compressor cavities under strong rotation. *Model* used here refers to both a theory or an experiment (usually operating at benign conditions and at a smaller scale) that simulates a physical system with some simplifications. Broadly, such modelling uses dimensional analysis to determine the dependence of observable parameters, often in the form of power-law exponents.

Buoyancy-induced rotating flows occur widely in geophysics, with phenomena in the earth's atmosphere similar to those in rotating cavities: both are influenced by temperature gradients (radial for cavities where the centripetal acceleration dominates or vertical for the atmosphere where gravity controls the thermal lapse rate), rotation and compressibility. Beyond applications to the atmosphere and technology, thermal convection is an omnipresent phenomenon in nature, including the circulation of the oceans (Ra ~ 10^{20}) and heat transport in the Sun (Ra ~ 10^{23}) – see Niemela *et al.* [7]. Heated rotating cavity experimental models have been used to create large Ra in the simulation of flows naturally governed by gravitational acceleration, *e.g.* Hide [16], in the context of fluid motion in the Earth's liquid core, and more recently Jiang *et al.* [17].

2 PLUME MODEL TO PREDICT HEAT TRANSFER FOR A CLOSED ROTATING CAVITY

In a closely-connected paper [18], Tang and Owen developed a quasi-axisymmetric conjugate model for buoyancy-induced flow in a closed rotating cavity; the radial variations of the temperature of the discs and fluid core, and that of the heat flux between the discs and the core, were predicted for compressible flow. The model assumed that radial plumes of fluid in the core convect heat from the hot shroud to the cold hub. In addition, heat transfer between the discs and the core occurs via Ekman layers on the discs, and the circular fin equation was used to calculate the conduction inside the discs [19]. The circular fin equation can be written as

$$\frac{d^2 T_d}{dr^2} + \frac{1}{r}\frac{dT_d}{dr} - \frac{2h}{t_d k_d}(T_d - T_c) = 0 \tag{11}$$

where T_d is the disc temperature, t_d the disc thickness, h the heat transfer coefficient, k_d the thermal conductivity of the disc material, and T_c the temperature of the core. A circumferential pressure gradient was assumed to exist in the

core, which was equivalent to the gradient created by the vortex pairs in the actual fluid; the pressure gradient was shown to be proportional to the mass flow rate in the plumes.

The core temperature, which was assumed to be intermediate between that of the hot and cold plumes, was shown to increase with increasing radius. The temperature increase was shown to depend not only on the heat transfer from the discs but also on a compressibility parameter, $\chi \overset{\text{def}}{=} \text{Ma}^2/\beta\Delta T$, where Ma is the Mach number of the rotating core, $\text{Ma} = \Omega b / [2\gamma R(T_b+T_a)]^{0.5}$. Here χ represents the ratio of temperature rise caused by compressibility effects to temperature differences between cavity shroud and hub. The model derives equations directly relating non-dimensional temperatures for the disc and core to three independent non-dimensional governing parameters: the rotational Reynolds number Re_ϕ, the buoyancy parameter $\beta\Delta T$, and the compressibility parameter χ. (Note that the Grashof number $(\text{Gr} = \text{Re}^2_\phi \beta\Delta T)$ could be used to replace either Re_ϕ or $\beta\Delta T$ as one of the three independent parameters.) A critical value of χ exists for which the core and shroud temperatures are equal; above this critical value, stratification is predicted to occur and heat transfer between the core and the shroud will be by conduction rather than by convection.

As buoyancy-induced heat transfer is a conjugate problem, where the heat transfer in the fluid and the solid are coupled, the relative effects of conduction and convection are related to the Biot number. The conduction in the discs can be determined experimentally using the heat flux obtained from the measured radial distribution of the disc temperature. However, the determination of heat flux from temperature measurements is an example of an *inverse problem*, where small uncertainties in the temperature measurements can create large uncertainties in the computed heat flux. In [19], Bayesian statistics were applied to the circular fin equation to produce reliable estimates of the Biot number and 95% confidence limits. This method was also used to successfully compute the Nusselt numbers, and their confidence intervals, using disc-temperature measurements from the Bath Compressor Cavity Rig [20]. The plume model requires only the measured temperatures at $r = a$ and $r = b$ to predict the disc and air temperatures. The Bayesian model uses the disc temperatures to derive experimental disc heat fluxes.

3 BATH COMPRESSOR CAVITY RIG

The experiments described below were conducted using the Bath Compressor-Cavity Rig, which simulates a generic axial compressor at fluid-dynamically scaled conditions. The rig was specifically designed to investigate buoyancy-induced heat transfer, generating data of practical interest to aero-engine designers and for the validation of theoretical and computational models. A thermal-mechanical stress analysis and detailed description of the instrumentation is provided by Luberti *et al.* [21]. An overview of the rig capability is provided here.

Figure 3 is an isometric view of the rig showing the test section as part of a disc drum forming three cavities. The disc drum is made of titanium alloy (Ti-5AL-4V, grade 5, annealed), and the thermal conductivity of the material at 293 K is 6.6 W/(m K) [22]. A closed cylindrical rotating annulus was created by attaching aluminium rings (highlighted red in

the figure) to the cobs in the central cavity. The disc drum was mounted on a spindle, driven using a belt and 30 kW motor to a maximum rotational speed of 8,000 rpm - equivalent to $\text{Re}_\phi = 3\times10^6$. Circular heater elements were used to control the temperature of the shroud up to 100 °C, equivalent to a buoyancy parameter $\beta\Delta T \sim 0.15$. To provide the necessary heat sink to cool the inner cylindrical surface of the closed cavity, ambient air was drawn through a bell-mouth inlet and passed axially between the bore of the discs and a stationary central shaft.

All measurements were conducted in the central, closed cavity under carefully controlled thermal boundary conditions. The surfaces of the two outer cavities and the back surfaces of the co-rotating titanium discs were insulated with Rohacell, a low thermal conductivity foam; this provided the near-adiabatic condition necessary to apply the Bayesian statistical methods to derive the disc heat fluxes. Unlike the Aachen rig (where the discs were quasi-adiabatic) there was significant heat transfer from the disc surfaces to the air in the rotating core. The surfaces of the discs, shroud and hub were painted matt black so the effects of radiation could be quantified [23].

Figure 4 shows the instrumented central cavity ($a/b = 0.45$ and $G = s/b = 0.17$) and inner cavity for the axial cooling throughflow. The geometric features include the cob, a section with a fillet radius to the constant-thickness diaphragm, and an outer fillet radius near the shroud. The shroud and hub radii are $b = 240$ mm and $a = 109$ mm, respectively. The constant-thickness disc diaphragm extends between radius $i = 124$ mm to $o = 235$ mm.

Sixty-four K-type thermocouples were directly embedded into circumferential grooves on the two rotating surfaces of the diaphragms and cobs forming the rotating cavity. The circumferential grooves were designed to span an isotherm at constant radius. The epoxy resin was specifically selected to
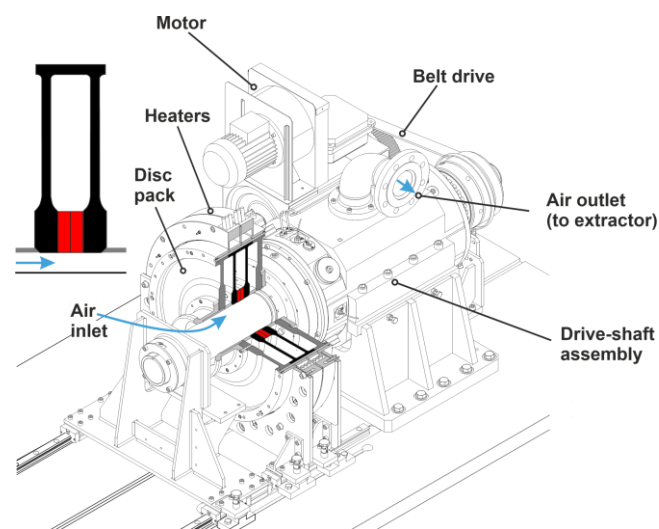

Figure 3: The experimental rig (designed in collaboration with Torquemeters Ltd.) showing a section view of the disc drum. The central cavity test section is shaded black and the aluminium rings are shaded red.

TURBO-22-1170-TANG

satisfy both adhesive criteria (sheer and peel strength) and match the thermal conductivity of titanium [21], leaving a hydraulically smooth surface.

An RdF thermopile heat flux gauge, with 54 thermopile junctions made from copper-constantan pairs, was used to directly measure the heat flux from the shroud. The dimensions of this gauge were 15 mm by 46 mm, spanning the full width along the underside of the downstream disc. The gauge was calibrated using a generic method described by Pountney *et al.* [24] where an equation based on physical properties was derived to establish the theoretical relationship between the measured voltage output of the gauge and the heat flux through it. A bespoke experimental rig was used to calibrate the gauge under steady-state conditions for heat fluxes $0.5 < q < 8$ kW/m^2. The temperature of the gauge was accurately controlled between 30 and 110°C, and a voltage-flux correlation (based on the theoretical relationship) was determined using Maximum Likelihood Estimation. MLE is a statistical method for estimating the value of parameters from a given data set, and details of the method are provided by Silvey [25] and Davison [26]. The equation used to determine the heat flux, q, was:

$$q = \frac{\tilde{k}V}{c(A_1 + 2A_2 T_g)} \quad (12)$$

where V is the measured voltage from the heat flux gauge, T_g the gauge temperature, and c the number of thermopile junctions. A_1, A_2, and $\tilde{k}$ are constants determined from the calibration.

Two fast-response unsteady pressure sensors (Kulite XCQ-080 series) were flush-mounted in the diaphragm of the downstream disc at $r/b = 0.85$. The sensors had a circumferential spacing of 35°. These were used to determine the cyclonic / anticyclonic flow structures in the rotating cavity. The method of spectral analysis, which provides the number of vortex pairs and the slip relative to the disc, is described by Jackson *et al.* [13].

All instrumentation wires were passed through the centre of the spindle to a Datatel telemetry unit. The data from the rotating frame were transmitted to a receiver via an antenna. The thermocouple signals were compensated using the cold junction temperature from an RTD (Resistance Temperature Detector) and converted to a temperature using a known calibration. As discussed in detail by Jackson *et al.* [20], the estimated combined uncertainty of the rotating thermocouples is ± 0.5 °C. The thermocouple measurements were sampled at 10 Hz. All data were collected in the steady state, defined as when the median average of the nondimensional disc temperature (defined below) for each disc thermocouple changed by less than 0.01 between a pair of ten-minute intervals. The fast-response pressure sensors were connected to a separate high-frequency transmitter module; these data were passed through a 1 kHz low-pass filter before being sampled at 10 kHz to minimize effects of signal aliasing. Jackson *et al.* [13] show that the combined uncertainty of the absolute pressure measurement is described by the standard deviation of ± 1.5 mbar. The shroud heat flux had a standard error between 2.5% and 4% of the measured value [27].

Definitions of key parameters

Tang and Owen [18] have conducted a parametric study to show the theoretical effect of the rotational Reynolds number Re_ϕ, the buoyancy parameter $\beta\Delta T$, compressibility parameter χ, and the thermal conductivity of the discs on the nondimensional core and disc temperatures, θ_c and θ_d. The nondimensional parameters and temperatures were defined as follows:

$$\text{Re}_\phi \overset{\text{def}}{=} \frac{\Omega b^2}{\nu} \quad (13)$$

$$\beta\Delta T \overset{\text{def}}{=} \frac{2\Delta T}{T_b + T_a} \quad (14)$$

$$\chi \overset{\text{def}}{=} \frac{\text{Ma}^2}{\beta\Delta T} \quad \text{where } \text{Ma}^2 = \frac{\Omega^2 b^2}{\gamma R(T_b + T_a)/2} \quad (15)$$

$$\theta_c \overset{\text{def}}{=} \frac{T_c - T_a}{\Delta T} \quad (16)$$

$$\theta_d \overset{\text{def}}{=} \frac{T_d - T_a}{\Delta T} \quad (17)$$

Here $\Delta T = T_b - T_a$ is the difference in the temperatures between the shroud and hub at radii b and a. The nondimensional radius is defined as $x = r/b$, with $x_a = 0.45$, $x_i = 0.52$ and $x_o = 0.98$ – see Figure 4. As shown by Tang and Owen [18], the radial distribution of θ_c is determined by the compressibility parameter χ, and the disc temperature can be calculated using the non-dimensional form of the circular fin equation:

$$\frac{d^2\theta_d}{dx^2} + \frac{1}{x}\frac{d\theta_d}{dx} - \text{Bi}(\theta_d - \theta_c) = 0 \quad (18)$$

where Bi is a modified Biot number. Assuming conduction dominates heat transfer in the Ekman Layers, Bi is defined and related to the rotational Reynolds number as

$$\text{Bi} \overset{\text{def}}{=} 2\left(\frac{b^2}{t_d^2}\right)\frac{h_d t_d}{k_d} = 2\left(\frac{b}{t_d}\right)\left(\frac{k}{k_d}\right)\text{Re}_\phi^{1/2} \quad (19)$$

Definitions of Gr$_B$ and Nu$_B$ based on the experiments of Bohn *et al.* [3] are given by eqs. 6 and 8. Experiments conducted using the Bath Compressor-Cavity Rig are presented below using these definitions as well as the definitions that use the calculated core temperature from the Tang and Owen plume model:

$$\text{Gr}_S \overset{\text{def}}{=} \frac{\Omega^2 b(s/2)^3 \beta(T_b - T_{c,b})}{\nu_{c,b}^2} \quad (20)$$

$$\text{Nu}_S \overset{\text{def}}{=} \frac{q_b(s/2)}{k_{c,b}(T_b - T_{c,b})} \quad (21)$$

Here $T_{c,b}$ is the theoretical air temperature of the core at radius b, and $s/2$ is used as the characteristic length L and $\beta^{-1} = (T_a + T_b)/2$. Other symbols are listed in the nomenclature. In total, 23 experiments were conducted across a range of $\beta\Delta T$ and Re_ϕ (and therefore, Gr if assuming $L = b$), with a summary of the dimensional and non-dimensional parameters

TURBO-22-1170-TANG

Case ID	A_1	A_2	A_3	B_1	B_2	B_3	C_1	C_3	D_1	D_2	D_3	E_0	E_1	E_2	E_3	F_0	F_1	F_2	F_3	G_0	G_1	G_2	G_3
N (k rpm)	2	2	2	3	3	3	4	4	5	5	5	6	6	6	6	7	7	7	7	8	8	8	8
$Re_\phi/10^6$	0.76	0.73	0.70	1.1	1.1	1.0	1.5	1.4	1.9	1.7	1.7	2.3	2.2	2.1	2.0	2.5	2.4	2.3	2.3	2.9	2.6	2.7	2.5
$\beta\Delta T$	0.07	0.10	0.14	0.07	0.11	0.13	0.07	0.14	0.07	0.10	0.13	0.03	0.07	0.10	0.13	0.04	0.07	0.10	0.13	0.06	0.08	0.10	0.13
$Gr/10^{11}$	0.41	0.55	0.68	0.91	1.3	1.4	1.6	2.5	2.5	3.0	3.8	1.6	3.5	4.5	5.3	2.5	4.0	5.7	6.8	4.7	5.9	7.7	8.4
Ma	0.14	0.14	0.13	0.21	0.21	0.20	0.28	0.27	0.35	0.34	0.34	0.44	0.42	0.41	0.40	0.50	0.49	0.48	0.47	0.57	0.54	0.55	0.53
χ	0.29	0.19	0.13	0.63	0.39	0.30	1.1	0.53	1.7	1.1	0.83	5.9	2.5	1.6	1.2	6.6	3.5	2.2	1.7	5.5	3.5	2.9	2.2
$Gr_B/10^{10}$	0.48	0.66	0.80	1.1	1.5	1.7	1.9	3.0	2.9	3.5	4.5	1.9	4.1	5.4	6.3	2.9	4.4	6.7	8.0	5.5	6.9	9.1	9.9
Nu_B	36	43	48	46	51	62	51	74	48	66	80	-0.17	39	65	83	-1.6	-	56	80	-0.18	-	47	69
$Gr_S/10^8$	0.11	0.15	0.17	0.24	0.32	0.34	0.40	0.57	0.55	0.69	0.86	-	0.66	0.97	1.2	-	0.67	1.1	1.4	-	1.0	1.3	1.6
Nu_S	7.1	8.0	8.8	9.6	10	12	12	15	13	15	17	-	13	17	20	-	-	18	21	-	-	18	21
n	3	3	3	3	3	3	3	3	3	3	3	0	3	3	3	0	4	4	3	0	4	4	4
$C_p \times 10^2$	1.7	2.2	2.6	1.6	2.2	2.5	1.6	2.4	1.5	1.9	2.4	0	1.2	1.8	2.2	0	0.7	1.6	2.1	0	0.8	1.4	1.9
$C_w/10^4$	1.9	2.5	2.7	2.8	3.6	3.8	3.6	4.9	4.1	4.9	5.9	0	4.1	5.8	6.7	0	3.4	7.5	7.0	0	4.4	7.7	9.8

Table 1: Parameter ranges for all test cases. (Letters in the case ID represent different rotational speeds and numbered subscripts show different levels of $\beta\Delta T$. Comparison between theory and experiment for all cases are shown in the appendix and cases discussed in the main content are denoted using bold fonts.)
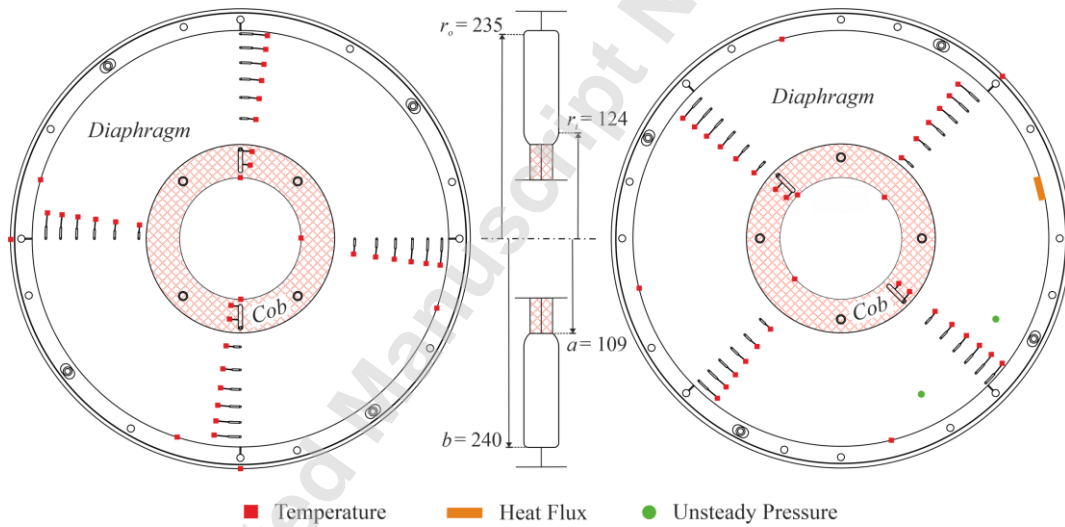

Figure 4: Instrumentation locations on the discs (radii in mm)

given in Table 1. The rig was limited to $0.063 < \beta\Delta T < 0.14$, $7.0 \times 10^5 < Re_\phi < 2.9 \times 10^6$ and $0.13 < \chi < 6.6$.

4 RADIAL VARIATION OF DISC AND CORE TEMPERATURES

Here the term *experimentally-derived values* refers to the temperatures and heat fluxes determined using the Bayesian model [19]; *theoretical values* refer to the temperatures and fluxes predicted from the Tang and Owen model [18]. The Appendix shows good agreement between the theoretical model and experimental measurements over a wide range of

Re_ϕ, $\beta\Delta T$ and χ. Four cases are discussed in detail in this section.

Figure 5a/b show the measured radial variation of non-dimensional disc temperature, comparing cases A_3 and G_3 (see Table 1) at constant $\beta\Delta T$ but at two Re_ϕ for low and high χ. The nondimensional radii of the cob, fillet to constant-thickness diaphragm, and outer fillet are marked. The disc temperature is nearly uniform across the aluminium hub (used to close the cavity) with an increase with increasing radius across the diaphragm of the titanium disc. Also presented across the diaphragm are the continuous temperature distributions derived from the Bayesian model

(dashed lines) with the 95% confidence intervals shown by the red/black fill.

In addition to these experimentally derived values are the theoretical predictions of both disc (solid line) and core (dotted line) temperatures. Due to the conjugate nature of the heat transfer in the closed cavity, these predictions were generated by solving the equation for the radial distribution of the core temperature and the fin equation (eq. 18) simultaneously. The core temperatures were determined using

$$\frac{d\theta_c}{dx} = \xi + (\gamma - 1)x\chi \qquad (22)$$

where ξ is the parameter used in the plume model to account for the effect of disc heat transfer on core temperatures. More details about the solution technique can be found in [18]. Solving the system of equations requires disc boundary conditions at x_i and x_o and core temperatures at x_i. The disc boundary conditions were taken to be the measured disc temperatures, and the core temperature at x_i (not measured) was optimised to provide the least-squares of the differences between the predicted and measured disc temperatures. The optimisation was realised using the trust-region-reflective gradient-based algorithm [28] and stopped when the change of core temperature at x_i is less than 10^{-3} degree.

The predictions show the effect of compressibility on θ_d and θ_c increases as χ increases; this could be significant at engine-operating conditions. There is a remarkable agreement between theory and experiments, with the disc

temperatures behaving as predicted. An inset provides more detail over a segment of the curve.

The theoretical nondimensional core temperature is strongly affected by χ. Compressibility effects are relatively small at low values of χ (0.13) and so is the corresponding radial increase of θ_c. At large values of χ (2.2), where the effects of compressibility are more significant, the temperature difference between the core and shroud decreases and consequently there is a reduction in heat transfer at high radius and an increase in θ_d.

The corresponding heat flux distributions across the diaphragm are shown in Figure 5c. The Bayesian model uses the measured temperatures to determine the *experimentally-derived* heat fluxes and their 95% confidence intervals, which are shown by dashed lines and red/black fill. As discussed in Section 2, plumes of air act as conduits of heat transfer between the hot shroud and cold hub, with radial movement being driven by their change in density. A negative flux indicates that heat is transferred from the air to the disc (*i.e.* the core is hotter than the disc at that radius); the reverse occurs for a positive flux. Also shown are the theoretical heat fluxes (solid lines), which all lie within the uncertainty range of the "*experimentally-derived*" heat fluxes.

It is difficult to identify the effect of χ on temperatures from cases A₃ and G₃ as both Re_ϕ and χ change. Therefore, Figure 6 shows the variation of disc and core temperatures while fixing Re_ϕ. Figure 6a shows the effect of χ on the radial variation of the temperature of the disc and core at a constant $Re_\phi \approx 2.5 \times 10^6$ (cases F₁ and F₃ in Table 1, $\chi = 3.5$ and 1.7). The measured and theoretical disc temperatures agree well
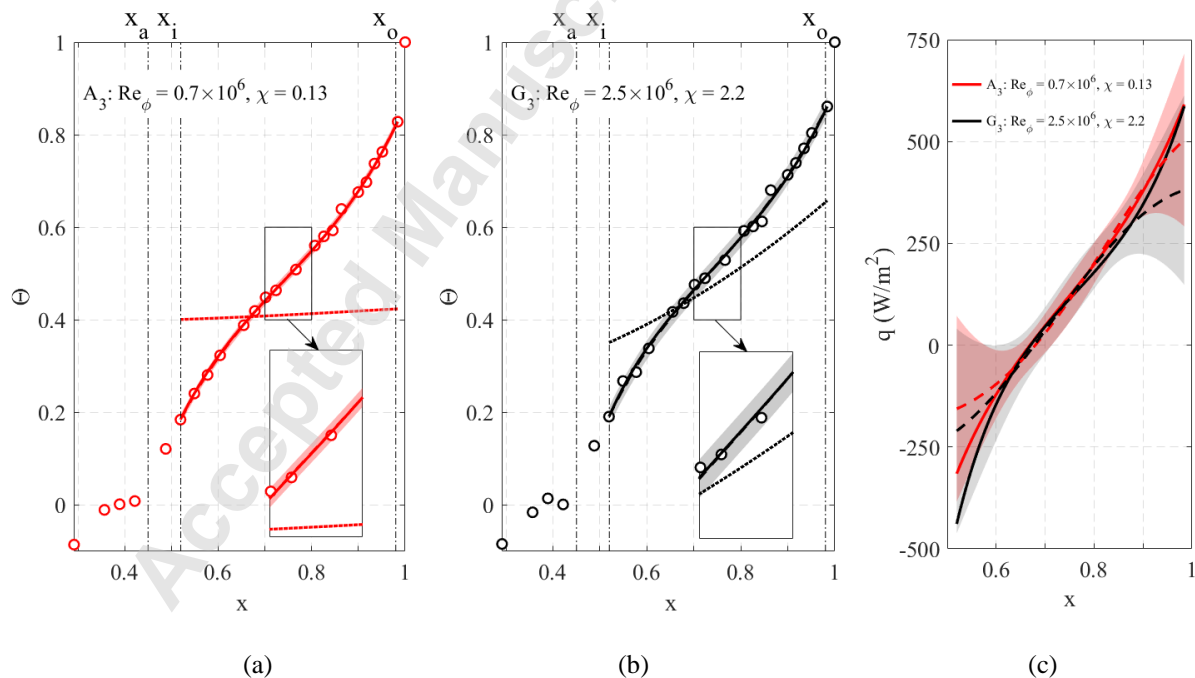

Figure 5: Effect of Re_ϕ and χ (a and b) on disc and core temperatures and (c) convective heat flux for $\beta\Delta T = 0.14$. Experiments: data pints and Bayesian dash line (shading shows 95% confidence intervals). Theory: solid line Θ_d and dotted line Θ_c.

TURBO-22-1170-TANG

and there is a clear measured effect of compressibility for $\chi = 3.5$ (case F_1). At the larger value of χ, the temperature of the core at high radii approaches that of the shroud. Figure 6b shows the corresponding heat flux distributions across the diaphragm. As discussed in [18] there will be a critical value of χ where the core and shroud temperature are equal, where it is speculated that stratification of the flow may start to occur.

5 SHROUD HEAT TRANSFER CORRELATIONS

From eqs. 6-8, the experimental values of Nu_B and Gr_B can be determined using the experimental values of shroud heat fluxes and shroud and hub temperatures. Here the flux was measured directly using the thermopile gauge and corrected for radiation. The shroud and hub temperatures were measured using thermocouples. Figure 7 illustrates the experimental measurements of shroud heat transfer. The effect of χ on the variation of Nu_B with Gr_B is shown for most cases in Table 1. (Not shown are cases E_0, F_0 and G_0, where the core is stratified and $Nu_B \sim 0$ as discussed in Section 7.) The correlations obtained by Bohn *et al.* [3] and Bohn and Gier [11] are also presented.

It should be noted that the definition of Nu_B in eq. 8 is based on the one-dimensional ratio of convection to conduction in the cavity. A quantitative comparison is only valid between rigs if the discs are adiabatic, and the axial width of the shroud and hub are equal. The discs are not adiabatic in the Bath rig used here and the axial width of the shroud and hub are unequal. Consequently, only a qualitative comparison with the one-dimensional correlation is possible.

Figure 7 shows that the increasing trend of measured heat transfer (or maxima) at a given $\beta \Delta T$ ends for $\chi > 1.1$. This is because as χ increases, the radial increase of the core temperature becomes significant and the temperature of the core at high radius approaches that of the shroud, reducing

the shroud heat transfer. The experiments in the Aachen rig were conducted with a maximum rotational speed of 3500 rpm and $\chi \approx 1.0$.

Figure 8 illustrates the experimental measurements of shroud heat transfer in the form of Gr_S and Nu_S, using eqs. 20 and 21. To determine this correlation, shroud heat fluxes and appropriate reference temperatures are required. The shroud heat flux was measured directly using the thermopile gauge and corrected for radiation [23]. The reference temperature was taken as $T_{o,c}$ the theoretical temperature of the core at radius r_o. A consistent trend is seen from all cases and the data were correlated by:

$$Nu_s = 0.010(Gr_s\ Pr)^{0.41} \qquad (23)$$

The statistical fit and confidence limits for this equation were determined using MLE. The 95% confidence limit of the fitted Nusselt numbers is ± 2.0. This shows a consistent shroud heat transfer correlation over a wide range of χ. The exponent 0.40 is higher than those found in flat plate free convection correlations (0.25 for laminar flow and 0.33 for turbulent).

The above has referred to closed cavity configurations for compressors. There are several published correlations for shroud heat transfer in open cavities with axial throughflow and the reader is directed to Jackson et al. [27] and Long and Childs [29].

6 CIRCUMFERENTIAL PRESSURE VARIATION IN THE ROTATING CAVITY

As discussed in Section 2, the Tang and Owen model [18] describes the mechanism for convective heat transfer between the heated shroud to the cold hub in terms of plumes of fluid at different temperatures. As shown in Figure 2, the cold fluid moves radially outward, and the hot fluid inward, inside a rotating inviscid core in which there are radial and circumferential distributions of pressure. Using the linear equation for tangential momentum, Tang and Owen linked the circumferential pressure variation with the non-dimensional mass flow rate of the plumes (C_w) in terms of the number of cyclonic and anti-cyclonic vortex pairs (n) and the difference in pressure (Δp) between the centre of the cyclonic and anticyclonic vortices:

$$C_w \overset{\text{def}}{=} \frac{\dot{m}}{\mu s} = \frac{n\text{Re}_\phi C_p}{2} \qquad (24)$$

$$C_p = \frac{\Delta p}{\rho \Omega^2 b^2} \qquad (25)$$

Here Δp is the maximum-to-minimum pressure difference between the vortex pairs. As discussed below, C_w has been correlated in terms of the Grashof number Gr_S.
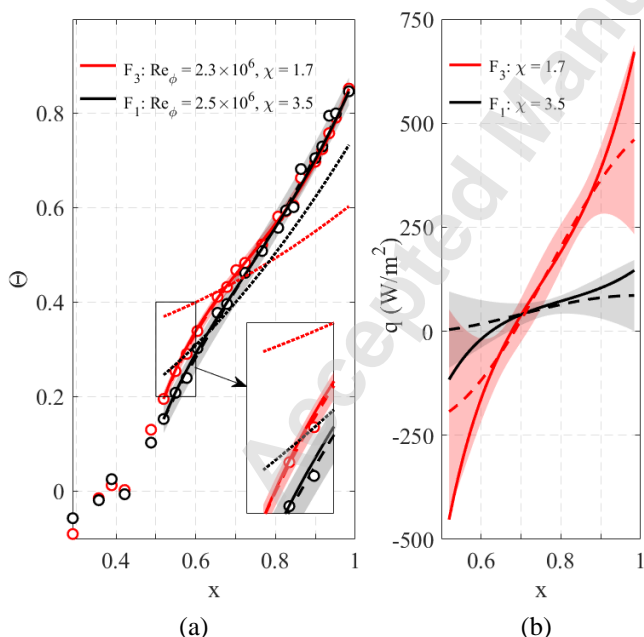
Figure 6: Effects of χ on (a) disc and core temperatures; (b) heat fluxes. Experiments: data points and Bayesian dashed line (shading shows 95% confidence intervals). Theory: solid line Θ_d and q and dotted line Θ_c.
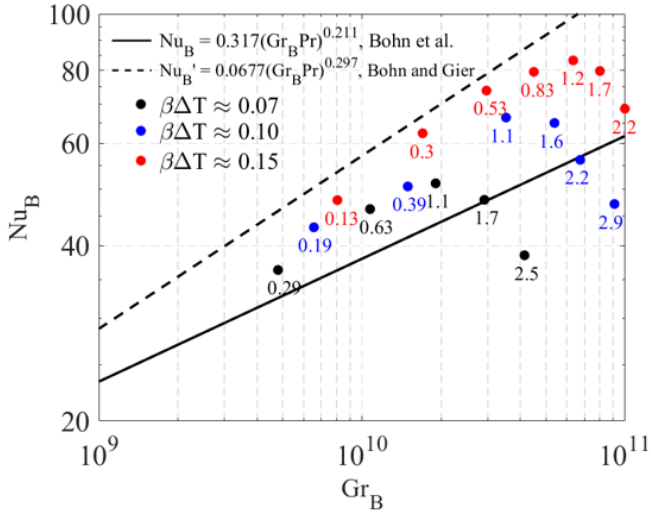
TURBO-22-1170-TANG

Figure 7: Effect of χ on the variation of Nu_B with Gr_B for experimental cases in Table 1. Also shown are the correlations from Bohn et al. [3] and Bohn and Gier [11] (numbers below symbols show χ).
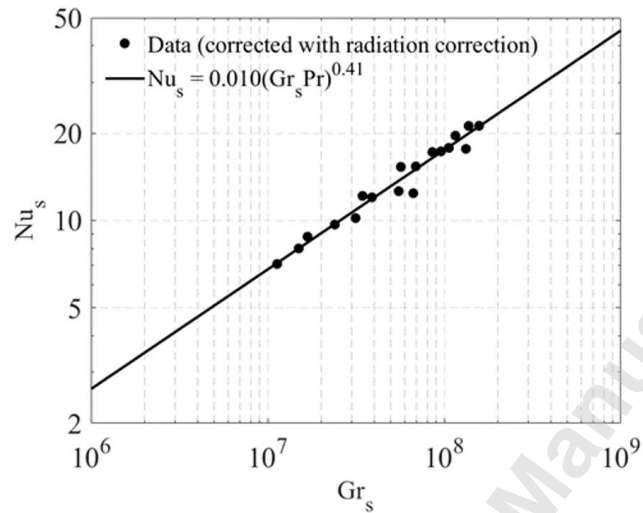

Figure 8: Experimental measurements of shroud heat transfer based on core temperature – see eqs. 20 and 21

Jackson et al. [13] used unsteady pressure sensors to detect either $n = 3$ or 4 rotating vortex pairs (depending upon Gr), with the fluid core slipping relative to the discs by < 1% of the disc speed. For the tests reported here, the two sensors were flush-mounted into the disc at $x = 0.85$ at a circumferential spacing of $\alpha = 35°$. Figure 9 is a conceptual sketch of the flow structure with three pairs of vortices. The angular speed of the structures is Ω_s, which can be determined as follows:

$$\Omega_s = \frac{\alpha}{\Delta t_\alpha} \qquad (26)$$

The time lag (Δt_α) between the two sensors was calculated from the peak of the cross-correlation between the two pressure signals and the number of vortex pairs determined from:

$$n = \frac{2\pi f_{s,1}}{\Omega_s} \qquad (27)$$

where $f_{s,1}$ is the passing frequency of one vortex pair, found from the Fast Fourier Transform (FFT) of the signal from either sensor. Table 1 listed the number (n) of vortex pairs at different experimental conditions. Four vortex pairs were detected for $Re_\phi > 2.5 \times 10^6$ while only three for $Re_\phi < 2.2 \times 10^6$. For $2.2 \times 10^6 < Re_\phi < 2.5 \times 10^6$, either $n = 3$ or 4 were detected. Note that details of the data sampling frequency are discussed in Section 3.

The magnitude of the maximum-to-minimum pressure difference between the vortex pairs (Δp) was determined by fitting a sinusoidal function to the pressure signals for each core structure revolution. The average values of Δp from all revolutions and both sensors were used to determine C_p for each case. The values of n and C_p are listed in Table 1 for all experimental cases. The data are plotted against the shroud Grashof number (Gr_S) in Figure 10. The data was fit to the following correlation

$$\frac{n Re_\phi C_p}{2} = 1.0(Gr_S Pr)^{0.61} \qquad (28)$$

The statistical fit and confidence limits for this equation were determined using MLE. The 95% confidence limit for the correlation is $\pm 1.45 \times 10^4$.

7 STRATIFIED FLOW

As discussed above, there will be a critical value χ_{crit} where the core and shroud temperatures are equal. Tang and Owen [18] speculated that under these conditions the fluid core will be stably stratified, where buoyancy-induced convection cannot occur and heat transfer from shroud to core is reduced to conduction. This large reduction of heat transfer, which could occur during an engine cycle, would have a significant effect on the temperature of the compressor discs.

Cases E_0, F_0 and G_0 in Table 1 reached $\chi > 5.5$ and the corresponding shroud heat flux (corrected for radiation) was measured to be virtually zero. Figure 11a shows the measured radial variation of non-dimensional disc temperature, comparing cases F_0 and F_3, at constant Re_ϕ but two $\beta\Delta T$ and consequently two values of χ. The higher value of $\chi = 6.6$ was the maximum obtainable (with reliable accuracy) using the rig. The continuous temperature distributions derived from
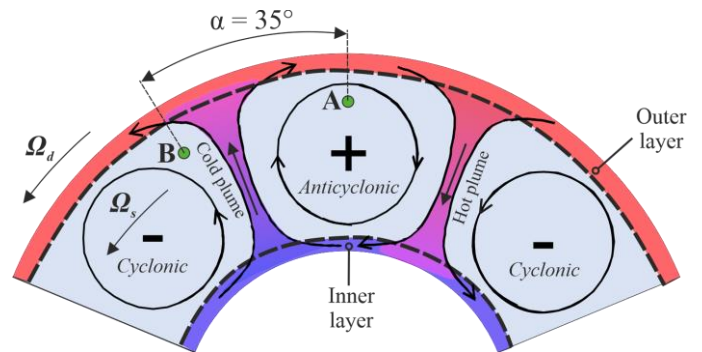

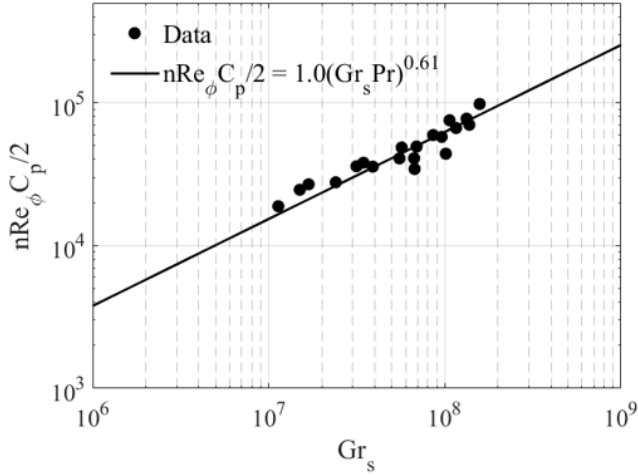**Figure 9: Flow structure in the r-ϕ plane showing three vortex pairs.**

Figure 10: Variation of $n\mathrm{Re}_\phi C_p/2$ with Gr_s for cases in Table 1. Symbols denote experimental measurements and the solid line the correlation using MLE.

the Bayesian model are shown as dashed lines, with the 95% confidence intervals shown by the shaded fill. The theoretical predictions of both disc (solid line) and core (dotted line) temperatures are shown for the case of $\chi = 1.7$; the theoretical model is invalid beyond χ_{crit} so no such curves are shown for $\chi = 6.6$.

The corresponding heat flux distributions from the Bayesian model are shown in Figure 11b. For case F_0, the radial distribution of convective heat flux is zero within experimental uncertainty and the disc temperature approaches the radial distribution corresponding to one-dimensional conduction in a cylinder:

$$\theta_d = \frac{\ln (x/x_i)}{\ln (x_o/x_i)} (\theta_{d,o} - \theta_{d,i}) + \theta_{d,i} \qquad (29)$$

As discussed above, two unsteady pressure sensors at $x = 0.85$ were used to determine the cyclonic / anticyclonic flow structure in the rotating cavity. The number of vortex pairs (n) were deduced from eq. 27. Figure 12 is an FFT of pressure signals for cases F_0, F_2 and F_3. For cases F_2 and F_3, the passing frequency of a single vortex pair, $f_{s,1}$, is shown by the peaks and ~ 1 - 2% the disc rotational frequency, f_d. The rotational frequency of the flow structure is $f_s = f_{s,1}/n$, with the difference between the disc and core rotation less than 1% of the disc speed (virtually solid-body rotation). Note the pressure coefficient in the FFT, $\widehat{C}_p$, is based on the difference between the static and mean of the data sample and differs from eq. 25. At a common value of Re_ϕ ~ 2.4 x 10^6 the magnitude of $\widehat{C}_p$ increases with Gr as buoyancy-induced convection intensifies. The slip of the structures is also seen to increase with Gr. For case F_0, these structures were not detected in the stratified core; as shown in Table 1, this was also observed for the other cases where $\chi > 5.5$ (E_0 and G_0).

Tang and Owen [18] calculated $\chi_{\mathrm{crit}} = 6.7$ for an ideal closed rotating cavity with insulated discs and $x_a = 0.5$ (*i.e.* similar to the experimental conditions here), though this value can be affected by disc heat transfer and cavity geometries.

Stratification may be considered a unique phenomenon if defined as the condition where the convective heat flux from the shroud reaches zero, and the buoyant cyclonic / anti-cyclonic structures disappear. However, for non-adiabatic discs the disc heat transfer can still be significant even if the shroud heat flux is zero. From this perspective stratification may be considered a *process*, with a critical radius (r^*) on the disc that divides the core between stratified ($r > r^*$) and buoyant ($r < r^*$) flow. Figure 13 shows the effect as $\chi \rightarrow \chi_{\mathrm{crit}}$ on the radial distribution of temperature across the disc. At high radius the temperature distribution for $\chi = 5.5$ is similar to that for $\chi = 6.6$ and eq. 29 but deviates from these curves at lower radii.
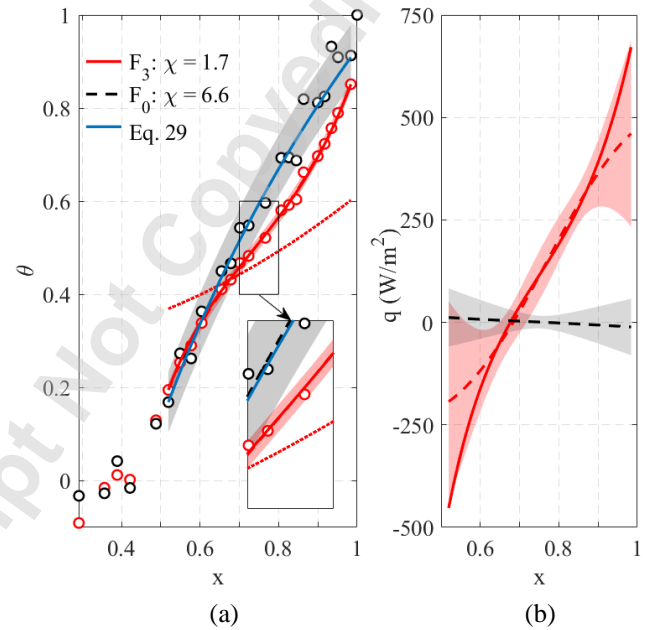

(a) (b)

Figure 11: Comparison of disc temperature and heat flux between cases F_0 and F_3. Experiments: data points and Bayesian dashed line (shading shows 95% confidence intervals). Theory: red solid line Θ_d and q and dotted line Θ_c. Temperature distribution from pure conduction using eq. 29: blue solid line.
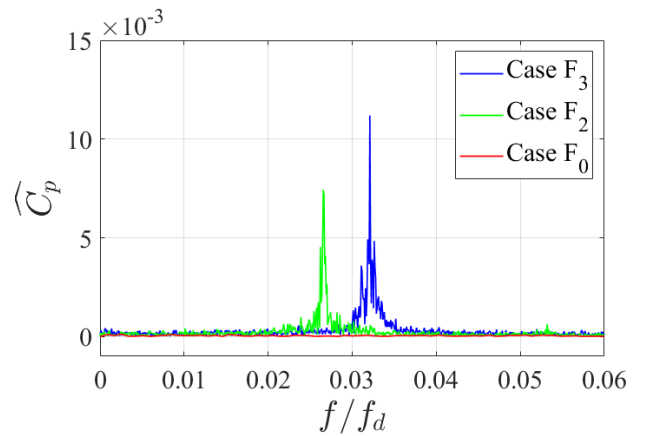

Figure 12: Effect of Gr and χ on the frequency spectra of the pressure measurements for Re_ϕ ~ 2.4x10^6.
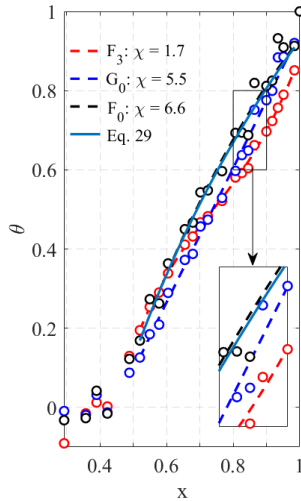
TURBO-22-1170-TANG

**Figure 13: Effect as $\chi \rightarrow \chi_{crit}$ on disc temperature.
Experiments: data points and Bayesian dashed line.
Temperature distribution from pure conduction using
eq. 29: blue solid line.**

Accurate and fast predictive methods are important for engine clearance decisions using combined thermo-mechanical models across the full operating flight envelope. This paper has considered steady-state scenarios. Under transient operating conditions, the relative expansion of the rotor and outer casing (both subjected to thermal and rotational growth, but with different inertia) influences the compressor tip clearance. The next phase of this research will address such transient behaviour.

8 CONCLUSIONS

Experiments have been conducted using a closed system of co-rotating discs where the heat transfer is driven by centrifugal buoyancy-induced flow. The results are compared with theoretical models and show the radial distribution of temperatures for the disc are governed by three independent, non-dimensional parameters: the rotational Reynolds number (Re_ϕ) the buoyancy parameter ($\beta \Delta T$), and the compressibility parameter of the rotating core (χ). The Grashof number (Gr = $Re^2_\phi \beta \Delta T$) could be used to replace either Re_ϕ or $\beta \Delta T$ as one of the three independent parameters. The experiments spanned $0.35 \times 10^6 < Re_\phi < 2.3 \times 10^6$, $0.08 < \beta \Delta T < 0.15$ and $0.07 < Ma < 0.56$, with the measured disc temperatures and heat fluxes agreeing closely with the theoretical distributions. The non-dimensional core temperature depends strongly on the magnitude of a compressibility parameter, $\chi \overset{\text{def}}{=} Ma^2/\beta \Delta T$, which is the ratio of temperature rise caused by compressibility effects to temperature differences between cavity shroud and hub. At large values of χ, where the effects of compressibility are significant, the fluid core at high radius will approach the shroud temperature. The experiments reveal for $Re_\phi = 2.6 \times 10^6$ a critical value $\chi_{crit} < 6.6$ where the convective heat flux to the shroud and discs is zero, and the radial distribution of disc temperature was that expected from pure conduction in a cylinder. Under such conditions, buoyancy effects are suppressed and the flow in the rotating cavity is stratified.

The influence of χ is also shown in shroud heat transfer correlations, which are compared qualitatively with previously published data collected where the effects of compressibility are relatively small. The heat transfer data were correlated as $Nu_S = 0.010\ (Gr_S\ Pr)^{0.41}$, based on the measured shroud heat flux and the theoretical core temperature. Sensors measuring unsteady pressure at $r/b = 0.85$ detected either $n = 3$ or 4 vortex pairs across the range of experimental conditions. These cyclonic and anti-cyclonic structures create the non-dimensional circumferential pressure difference (C_p) necessary for the radial inflow and outflow (of hot and cold fluid, respectively) within the rotating core. The magnitude of $nRe_\phi C_p/2$ is theoretically related to the nondimensional radial mass flow in the core, and the experiments show this flow rate can be correlated against Gr_S. Fast Fourier Transforms and cross-correlation of the unsteady pressure signals showed the fluid core slipped relative to the discs by less than 1% of the disc speed. These unsteady flow structures are associated with buoyancy-induced flow and were not detected under stratified conditions.

NOMENCLATURE

a	inner radius of cavity (hub) [m]
A_1, A_2	heat flux gauge calibration constants
b	outer radius of cavity (shroud) [m]
c	number of thermopile junctions
f_d	rotational frequency of discs [Hz]
f_s	rotational frequency of the flow structure [Hz]
$f_{s,1}$	passing frequency of one vortex pair [Hz]
G	cavity gap ratio
g	gravitational acceleration [m/s²]
h	heat transfer coefficients
i	inner radius of constant-thickness disc diaphragm [m]
k	thermal conductivity [W/mK]
$\tilde{k}$	heat flux gauge calibration constant
L	length scale [m]
$\dot{m}$	mass flow rate [kg/s]
n	number of vortex pairs
N	rotational speed of discs [rpm]
o	outer radius of constant-thickness disc diaphragm [m]
p	static pressure [Pa]
q	heat flux [W/m²]
R	gas constant
r	radius [m]
s	cavity width [m]
t	thickness [m]
T	temperature [K]
V	voltage [V]
x	nondimensional radial location
α	angular separation of unsteady pressure sensors [rad]
β	volume expansion coefficient [K⁻¹]
γ	ratio of specific heats
ρ	density [kg/m³]
μ	dynamic viscosity [kg/ms]
v	kinematic viscosity [m²/s]

TURBO-22-1170-TANG

Δt	time lag between unsteady pressure sensors [s]
Ω	angular velocity of disc [rad/s]
Ω_s	angular velocity of rotating structures [rad/s]

Dimensionless parameters

Bi	Biot number
C_p	pressure coefficient
$\widehat{C}_p$	pressure coefficient based on difference between static and mean pressures
C_w	flow coefficient
Gr	Grashof number
Ra	Rayleigh number
Re	Reynolds number
Re_ϕ	rotational Reynolds number
$\beta\Delta T$	buoyancy parameter
θ	non-dimensional temperature
χ	compressibility parameter
ξ	parameter used in the plume model to calculate θ_c $\left(= 4\pi^2 x \left(\frac{b}{s}\right)^2 \frac{\mathrm{Nu_d Nu_s}}{C_w^2 \mathrm{Pr}^2}\left[1 - \theta_{c,b} + \int_x^1 x \frac{\mathrm{Nu_d}}{\mathrm{Nu_s}}(\theta_d - \theta_c)dx\right]\right)$
Pr	Prandtl number
Nu	Nusselt number
Ma	Mach number

Subscripts and superscripts

|	
$a; i; b; o$	values at $r = a$; $r = $ i; $r = b$; $r = o$
B	Bohn
c	value in the fluid core
$crit$	critical
d	value of disc
g	gauge
s	value on shroud
ϕ,r,z	circumferential, radial and axial direction
*	stratification boundary

ACKNOWLEDGEMENTS

REFERENCES

[1] Owen, J. Michael, Hui Tang, and Gary D. Lock. 2018. "Buoyancy-Induced Heat Transfer inside Compressor Rotors: Overview of Theoretical Models" Aerospace 5, no. 1: 32.

[2] Tritton, D.J. 1988, "Physical Fluid Dynamics" OUP, New York.

[3] Bohn, D., Deuker, E., Emunds, R., and Gorzelitz, V. "Experimental and theoretical investigations of heat transfer in closed gas-filled rotating annuli", J. Turbomach. 1995, 117, 175–183.

[4] Tang, H., and Owen, J. M., 2018, "Theoretical Model of Buoyancy-Induced Heat Transfer in Closed Compressor Rotors", ASME J. Eng. Gas Turbines Power, 140(3), p. 032605.

[5] Pitz, D. B., Chew, J. W., Marxen, O., and Hills, N. J., 2017, "Direct Numerical Simulation of Rotating Cavity Flows Using a Spectral Element-Fourier Method", ASME J. Eng. Gas Turbines Power, 139(7), p. 072602.

[6] Holland, K. G. T., Raithby, G. D., and Konicek, L., 1975, "Correlation Equations for Free Convection Heat Transfer in Horizontal Layers of Air and Water", Int. J. Heat Mass Tran., 18(7–8), pp. 879–884.

[7] Neimela, J.J. Skrbek, L., Sreenivaasan, K.R., and Doonelly, R.J., 2000, "Turbulent Convection at Very High Rayleigh umbers", Nature 404, 837-840

[8] Grossmann, S., and Lohse, D., 2000, "Scaling in Thermal Convection: A Unifying Theory", J. Fluid Mech., 407, pp. 27–56.

[9] Pitz, D. B., Chew, J. W., and Marxen, O., 2019, "Large-Eddy Simulation of Buoyancy-Induced Flow in a Sealed Rotating Cavity", ASME J. Eng. Gas Turbines Power, 141(2), p. 021020.

[10] Gao, F., Pitz, D. B., and Chew, J. W., 2020, "Numerical Investigation of Buoyancy-Induced Flow in a Sealed Rapidly Rotating Disc Cavity", Int J. Heat Mass Tran., 147, p. 118860.

[11] Bohn, D., and Gier, J., 1998, "The Effect of Turbulence on the Heat Transfer in Closed Gas-Filled Rotating Annuli for Different Rayleigh Numbers", Proceedings of the ASME 1998 International Gas Turbine and Aeroengine Congress and Exhibition. Volume 4: Heat Transfer; Electric Power; Industrial and Cogeneration. Stockholm, Sweden. June 2–5, 1998. ASME 98-GT-542.

[12] Saini, D., Cheung, D., and Sandberg, R., 2018, "Direct Numerical Simulations of Centrifugal Buoyancy Induced Flow in a Closed Rotating Cavity", 21st Australasian Fluid Mechanics Conference.

[13] Jackson, R. W., Tang, H., Scobie J. A., Owen J. M. and Lock G. D., 2021, "Measurement of Heat Transfer and Flow Structures in a Closed Rotating Cavity", Proceedings of the ASME Turbo Expo 2021: Turbomachinery Technical Conference and Exposition. Volume 5B: Heat Transfer — General Interest; Internal Air Systems; Internal Cooling. Virtual, Online. June 7–11, 2021. GT2021-59605

[14] Owen, J. M., 2010, "Thermodynamic Analysis of Buoyancy-Induced Flow in Rotating Cavities", ASME. J. Turbomach., 132(3): 031006.

[15] Pitz, D., Marxen, O., & Chew, J., 2017, "Onset of Convection Induced by Centrifugal Buoyancy in a Rotating Cavity", Journal of Fluid Mechanics, 826, 484-502.

[16] Hide, R, 1958, "An Experimental Study of thermal Convection in a Rotating Fluid", Phil. Trans. R. Soc. London, A250, 441-478.

[17] Jiang, H., Zhu, X. Wang, D, Huisman, S.G., and Sun, C., 2020, "Supergravitational Turbulent Thermal Convection", Sci. Adv. 6: eabb8676.

[18] Tang, H and Owen, J.M., 2022, "Plume Model for Buoyancy-Induced Flow and Heat Transfer in Closed Rotating Cavities", ASME GT2022-80477.

[19] Tang, H., Shardlow, T., and Owen, J. M., 2015, "Use of Fin Equation to Calculate Nusselt Numbers for

TURBO-22-1170-TANG

Rotating Discs", ASME. J. Turbomach., 137(12), p. 121003.

[20] Jackson, R., Luberti, D., Tang, H., Pountney, O., Scobie, J., Sangan, C., Owen, J. M., and Lock, G. D., 2020, "Measurement and Analysis of Buoyancy-Induced Heat Transfer in Aero-Engine Compressor Rotors", ASME. J. Eng. Gas Turbines Power, 143(6): p. 061004.

[21] Luberti, D., Patinios, M., Jackson, R., Tang, H., Pountney, O., Scobie, J., Sangan, C., Owen, J. M., and Lock, G. D., 2020, "Design and Testing of a Rig to Investigate Buoyancy-Induced Heat Transfer in Aero-Engine Compressor Rotors", ASME. J. Eng. Gas Turbines Power, 143(4): p. 041030.

[22] G. Welsch, R. Boyer, and E. W. Collings, 1994, "Materials Properties Handbook: Titanium Alloys", ASM International.

[23] Tang, H., and Owen, J. M., 2020, "Effect of Radiation on Heat Transfer Inside Aeroengine Compressor Rotors", ASME. J. Turbomach., 143(5): p. 051005.

[24] Pountney, O., Patinios, M., Tang, H., Luberti, D., Sangan, C., Scobie, J., Owen, J. M., and Lock, G. D., 2021, "Calibration of Thermopile Heat Flux Gauges Using a Physically-Based Equation", Proceedings of the Institution of Mechanical Engineers, Part A: Journal of Power and Energy, vol. 235, no. 7, pp. 1806–1816.

[25] Silvey S.D. *Statistical Inference*. Chapman and Hall, London, 1975.

[26] Davison A.C. *Statistical Models*. Cambridge University Press, Cambridge, 2003.

[27] Jackson, R., Tang, H., Pountney, O., Scobie, J., Sangan, C., Owen, J. M., and Lock, G. D., 2021, "Analysis of Shroud and Disk Heat Transfer in Aero-Engine Compressor Rotors", ASME J. Eng. Gas Turbines Power, 143(9): p. 091005.

[28] Coleman, T.F. and Y. Li., 1996, "An Interior, Trust Region Approach for Nonlinear Minimization Subject to Bounds", SIAM Journal on Optimization, vol. 6, pp. 418–445.

[29] Long, C.A. and Childs, P.R.N., 2007, "Shroud Heat Transfer Measurements Inside a Heated Multiple Rotating Cavity with Axial Throughflow", Int. J. Heat Fluid Flow, 28 (6), pp1405-1417.

APPENDIX

Figure 14 presents the experimental and theoretical distributions of disc and core temperatures at fixed Re_ϕ but different $\beta\Delta T$ (hence different χ). There is good general agreement between experiment and theory.
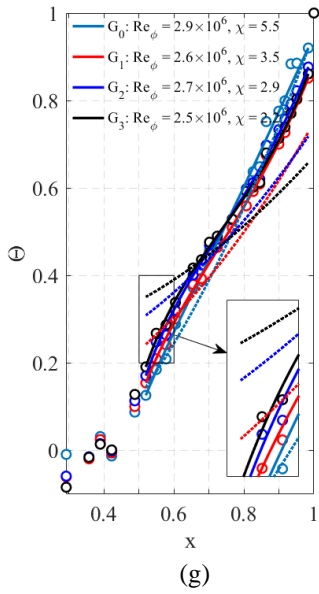
TURBO-22-1170-TANG

(g)
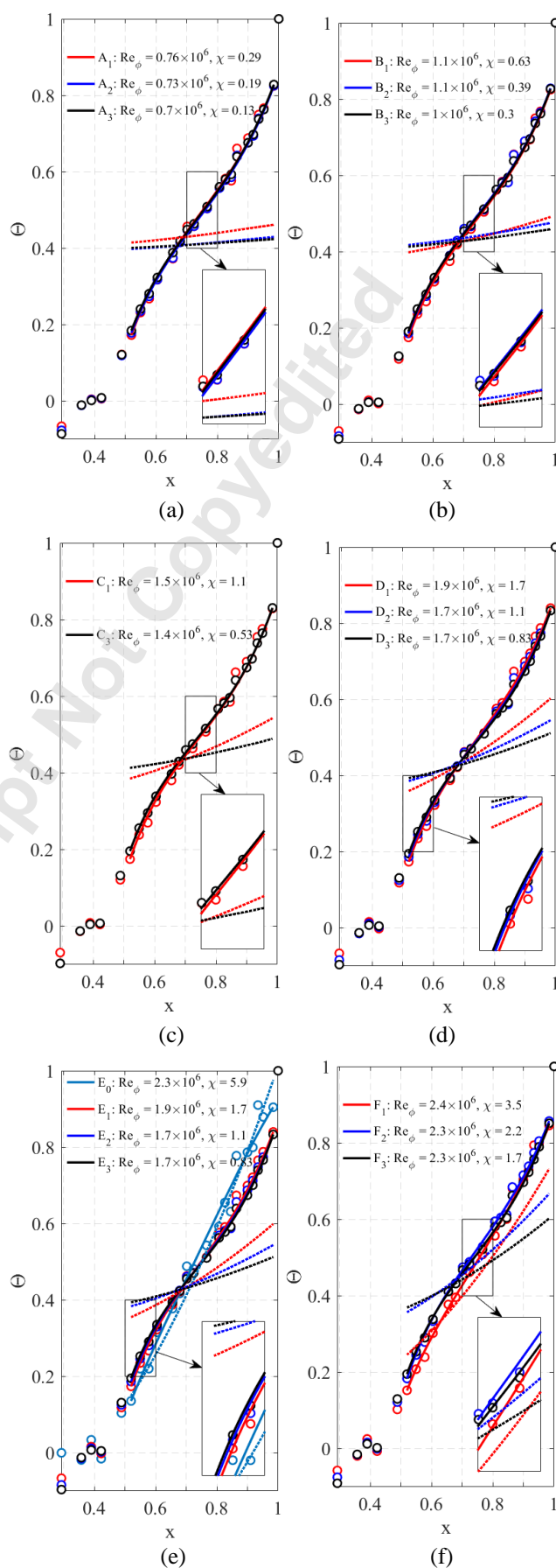
Figure 14: Theoretical and experimental disc and core temperatures for cases grouped by Re$_\phi$. Experiments: data points and Bayesian dashed line (shading shows 95% confidence intervals). Theory: solid line Θ_d and dotted line Θ_c .

TURBO-22-1170-TANG